

Coexistence of two order parameters and a pseudogap in the iron-based superconductor $\text{LaFeAsO}_{1-x}\text{F}_x$

R.S. Gonnelli¹, D. Daghero¹, M. Tortello¹, G.A. Ummarino¹, V.A. Stepanov², J. S. Kim³, and R. K. Kremer³.

¹ *Dipartimento di Fisica and CNISM, Politecnico di Torino, corso Duca degli Abruzzi 24, 10129 Torino (TO) – Italy*

² *P.N. Lebedev Physical Institute, Russian Academy of Sciences, Leninskiy Prospekt 53, 119991 Moscow, Russia*

³ *Max-Planck-Institut für Festkörperforschung, D-70569 Stuttgart, Germany*

The determination of the order parameter (OP) and its symmetry has always been of crucial importance in the study of superconducting materials ^{1,2}. The recent discovery of high-temperature superconductivity in $\text{XFeAsO}_{1-x}\text{F}_x$ with T_c ranging from 26 K ($X=\text{La}$) ³ to 43-55 K ($X= \text{Sm}, \text{Nd}$) ^{4, 5} poses important questions on the origin of the electron pairing in these compounds. While the standard electron-phonon mechanism seems ruled out ⁶, an unconventional, spin-fluctuation mediated pairing has been proposed ⁷. However, the nature and the precise value of the order parameters in these materials are still a matter of debate ⁸⁻¹³. Here we show that point-contact Andreev-reflection experiments on $\text{LaFeAsO}_{1-x}\text{F}_x$ give direct evidence of three energy scales in the superconducting state: i) a nodeless superconducting OP, $\Delta_1 = 2.8\text{-}4.6$ meV, scaling with the local T_c of the contact; ii) a larger unconventional OP (possibly of non-superconducting origin) that gives conductance peaks at 9.8-12 meV, apparently closes below T_c and disappears for $T_c \approx 31$ K; iii) a pseudogap surviving in the normal state up to $T^* \sim 140$ K (close to the Neel temperature of the undoped compound), which we associate to the presence of antiferromagnetic spin fluctuations (AF SF). This last finding indicates that AF SF coexist with superconductivity in $\text{LaFeAsO}_{1-x}\text{F}_x$. These results and their analogy with old and recent findings in superconductors like $\text{Ba}_{0.6}\text{K}_{0.4}\text{Fe}_2\text{As}_2$ ¹⁴, high- T_c cuprates ¹⁵ and URu_2Si_2 ¹⁶ prove the complex, strongly unconventional, nature of superconductivity in Fe-As-based superconductors.

The La-based oxypnictide $\text{LaFeAsO}_{1-x}\text{F}_x$ displays superconductivity with T_c up to 26 K for F contents $x = 0.05-0.12$ (Ref. 3), further increased in heavily-doped samples grown at high pressure¹⁷. The conventional phonon-mediated coupling mechanism cannot explain this high T_c ⁶ and the possible coupling mechanism is still debated.

Direct measurements of the superconducting order parameter (OP) are of crucial importance in this context. Point-contact spectroscopy (PCS) allows the determination of the OP also in present-day polycrystalline samples. The standard PCS technique consists in pressing a sharp metallic tip against the sample under study so as to obtain a small-size contact through which a probe current I is injected in the sample. Thanks to the quantum effect called Andreev reflection (see Ref. 9 and the relevant Supplementary Information), which takes place at the metal/superconductor interface, the differential conductance curve of the contact, dI/dV vs. V (V being the voltage across the junction) contains information about the amplitude and the symmetry of the OP. PCS measurements have been indeed recently carried out in $\text{LaFeAsO}_{1-x}\text{F}_x$ (Ref. 8), but also in $\text{SmFeAsO}_{1-x}\text{F}_x$ (Ref. 9,12), in oxygen-deficient $\text{NdFeAsO}_{0.85}$ (Ref. 10) and in $\text{NdFeAsO}_{0.9}\text{F}_{0.1}$ (Ref. 11).

Here we report on PCS measurements in polycrystalline samples of $\text{LaFeAsO}_{1-x}\text{F}_x$ by using a point-contact technique in which the counterelectrode is a small spot ($\varnothing < 50 \mu\text{m}$) of conducting paste containing micrometer-size Ag grains¹⁸ (see Supplementary Information for details). The actual contact area is thus by various orders of magnitude smaller than the apparent one. The $\text{LaFeAsO}_{1-x}\text{F}_x$ samples were grown according to Ref. 19 and present large (5-20 μm) crystallites in a more disordered matrix. The samples have nominal F content $x = 0.1$ and resistivity measurements show that bulk superconductivity sets in at $T_c \approx 27$ K, with a transition width of about 3 K. The local F content, as measured by micro-EDX (energy-dispersive X-ray spectroscopy) is uniform within the crystallites but can vary from one to another (with a spread $\Delta x = 0.02$). This will be reflected in a variation of the local critical temperature of the point contacts as well as of the order parameters.

Figure 1 reports three representative examples of raw point-contact conductance curves as a function of temperature, up to the normal state (thick line). All the curves show two symmetric peaks at low bias, plus additional structures (peaks or shoulders) at a higher voltage. Their shape indicates the presence of two order parameters, Δ_1 and Δ_2 , with nodeless symmetry – since, in a polycrystalline sample, the d -wave symmetry would result in a systematic observation of zero-bias conductance peaks that are not present in our curves. The existence of multiple OPs has been

recently proposed, for this material, on the basis of critical-field measurements²⁰, and it could well be compatible with the Fermi surface, made up of separate sheets²¹: recent angle-resolved photoemission spectroscopy (ARPES) measurements in $\text{Ba}_{0.6}\text{K}_{0.4}\text{Fe}_2\text{As}_2$ have indeed shown the opening of different OPs on the various sheets of the Fermi surface, which might be a general property of the Fe-As-based superconductors¹⁴. In all the conductance curves of Figure 1 the normal state is concave, with a systematic asymmetry⁹ probably related to the fast decrease in the density of states on crossing the Fermi level²¹.

If we suppose a superconducting origin for both the OPs, their amplitudes can be obtained from a fit of the experimental data with a suitable two-channel model for tunnelling spectroscopy in which the normalized point-contact conductance G is the weighted sum of two BTK contributions²², generalized to take into account broadening effects^{23,18} and the angular distribution of the injected current at the interface²⁴: $G = w_1 G_1^{\text{BTK}} + (1-w_1) G_2^{\text{BTK}}$. The parameters of this model – that we will call “generalized two-band BTK model” – are the OPs Δ_1 and Δ_2 , the potential barrier parameters Z_1 and Z_2 , the broadening parameters Γ_1 and Γ_2 , plus the weight w_1 . Prior to this fitting procedure, the normalization (i.e. division by the “normal-state” conductance, when $\Delta_1=\Delta_2=0$) must be performed. Here the normal state conductance at $T < T_c$ is not directly measurable because of the very high magnetic field necessary to suppress Δ_1 and Δ_2 , therefore some assumptions about its possible shape had to be made. We used here two different normalizations that are discussed in Supplementary Information, which also shows their modest effect on the OP amplitudes obtained from the fit.

Fig.2a shows an example of normalized conductance curves (symbols) compared to the relevant fit (lines) as a function of temperature (the raw data are those shown in Fig.1a). The resulting OP values are reported in panel b as full symbols. Their decrease on increasing the temperature, although regular and smooth, is definitely non-conventional. The larger OP, Δ_2 , actually shows a BCS-like behaviour up to about 22 K but, above this temperature, it either disappears or becomes so small that it is impossible for the measurement to discern it. The smaller OP, Δ_1 , follows a non-BCS temperature dependence with a “tail” up to the critical temperature of the contact, when the normal-state conductance is recovered. This is a quite general behaviour that has been observed in all the contacts we measured (another example is shown in Supplementary Information, that also reports the temperature dependence of the other fitting parameters). The same behaviour is obtained if only the small OP structures are fitted, disregarding the structures related to Δ_2 .

To collect further evidence for the presence of two OPs in $\text{LaFeAsO}_{1-x}\text{F}_x$ we also studied the magnetic field dependence of the PCS conductance curves, as shown in Fig.2c, where the experimental normalized conductance (symbols) is compared to the relevant fit (lines). The OPs extracted from the fit are reported in Fig. 2d as a function of the magnetic field intensity (full symbols). The different slope of the two trends (roughly linear, on this scale) indicates that Δ_2 is more sensitive to the magnetic field, possibly disappearing at a field of the order of 20 T.

The main question arising from the results shown so far is whether Δ_1 and Δ_2 are both superconducting OPs or, instead, one of them has a different origin. There is a number of experimental facts that find a simpler explanation if one admits that Δ_2 is not a superconducting OP: i) the anomalous temperature dependence, with the large OP Δ_2 apparently closing at $T < T_c$; ii) the very high value of the ratio $2\Delta_2(0)/k_B T_c \approx 8$; iii) the faster decrease of Δ_2 in magnetic field. The first two findings find no explanation within the standard two-band Eliashberg model²⁵ even if a weak (very strong) coupling and a very large (small) effective boson frequency are used for the band related to Δ_1 (Δ_2). If the larger OP is not superconducting, the normalized point-contact conductance must be modelled as the weighted sum of a BTK contribution (containing Δ_1 , Γ_1 and Z_1), and of a contribution from plain tunnelling into a density of states (DOS) featuring peaks whose energy scale Δ_{peak} is determined by the larger OP: $G = w_1 G_1^{\text{BTK}} + (1-w_1) G_2^{\text{tunn}}$. Hence, the latter contribution can be calculated as $G_2^{\text{tunn}} = (G - w_1 G_1^{\text{BTK}})/(1-w_1)$ being G the normalized experimental conductance curve and G_1^{BTK} the generalized single-band BTK conductance already used in the previous fit. For example, starting from the curves of Figure 2a one obtains the G_2^{tunn} curves reported in Figure 2e. The position of their peaks, indicated by arrows in Figure 2e, are reported in Figure 2b as blue open symbols. The same is done in Fig. 2d. Both the G_2^{tunn} curves and the temperature dependence of Δ_{peak} are strikingly similar to the findings of ARPES concerning the largest order parameter in $\text{Ba}_{0.6}\text{K}_{0.4}\text{Fe}_2\text{As}_2$ ¹⁴. This similarity points towards a general picture for Fe-As based superconductors, with two OP opening on different sheets of the FS: the smaller more or less BCS in value, and the larger strikingly non-BCS. The temperature at which the latter closes and its relationship with T_c seem to be rather sensitive to the exact material structure, which is consistent with the magnetic properties also being very sensitive to the details of the inner layer (between the Fe-As layers). This could indicate that the larger OP has a magnetic origin. However,

the possibility that it is a superconducting OP with a strongly unconventional behaviour, or it is at least coupled to superconductivity, cannot be completely rejected at the present stage of knowledge.

The different local F content in the crystallites gives rise to a distribution in local T_c values (already evident in Fig. 1) but also affects the OP values. Fig. 3a reports the normalized conductance of a 15- Ω contact with $T_c = 31.0$ K, showing only one OP. The fit of these curves with a generalized *single*-band BTK model (with only Δ , Γ and Z as parameters) gives the OP values reported in panel b. In this case the different normalizations discussed in Supplementary Information give Δ values that, at any temperature, differ by less than 10%. The ratio $2\Delta(0)/k_B T_c$ is equal to 3.44 – close to the standard BCS value for weak coupling in s-wave – but the temperature dependence is non-BCS and features the characteristic tail already observed in Fig.2b. The presence of a single OP is also shown by the magnetic-field dependence of the conductance curves (Fig. 3c) and by the corresponding plot of Δ as a function of the field (Fig.3d). A fit of these points (solid line) with a function $\Delta(B) = \Delta(0) \sqrt{1 - \frac{B}{B_{c2}}}$ (as expected for a bulk type-II superconductor^{1,2}) would lead to $B_{c2} \approx 55$ T, in reasonable agreement with direct critical-field measurements²⁰.

The values of Δ_1 and Δ_2 (and of Δ_{peak} if the larger OP is supposed to be non-superconducting) obtained in contacts with different local T_c are reported as a function of the T_c itself in Fig. 3e. A picture emerges in which Δ_1 slightly increases with T_c while Δ_2 (Δ_{peak}) quickly decreases, until a single, superconducting order parameter with BCS value is observed in the highest- T_c contact. The decrease of Δ_2 (Δ_{peak}) on increasing T_c further indicates that this OP may not be superconducting – although possibly coupled to superconductivity. If the critical temperature is related to the effective local F content, Fig. 3e can be converted in a phase diagram for the $\text{LaFeAsO}_{1-x}\text{F}_x$ compound, where the Δ_2 (Δ_{peak}) behaviour strongly reminds that of the pseudogap in high- T_c cuprates¹⁵.

To investigate the evolution of the normal-state conductance with temperature, we measured it up to $T \approx 200$ K, also expanding the voltage range up to about 100 mV. The results for two contacts are shown in Figure 4; note that panel b refers to the contact with the highest T_c . The normal state at T_c (upper thick line) is asymmetric and pseudogapped, with two broad maxima that are progressively smoothed out on increasing the temperature. This shape is very similar to that observed by PCS in materials with long-range spin-density-wave (SDW) order, like URu_2Si_2 ¹⁶. No such long-range SDW order was observed in superconducting $\text{LaFeAsO}_{1-x}\text{F}_x$ by neutron scattering or muon spin relaxation studies^{26,27}; however, these techniques can only detect quasi-static magnetic

order while photoemission and tunnelling (or Andreev-reflection) spectroscopies, being sensitive to electron dynamics, can detect phenomena on a much shorter time scale. On the other hand, the proximity of the superconducting state to the antiferromagnetic (AF) SDW state of the parent compound²⁸ suggests the persistence, in the doped compound, of spin fluctuations that have already been invoked as the origin of the pseudogap²⁹ also observed by photoemission spectroscopy^{13,29} in the same material. This picture has been recently substantiated theoretically by showing that, in systems with reduced dimensionality ($< 3D$), local AF fluctuations, even on a short range, can give rise to corrections in the self-energy of quasiparticles that, in turn, allow a pseudogap to be opened at the Fermi level³⁰. In this regard, it is very interesting to note that the pseudogap we directly observed in our conductance curves is progressively filled on increasing the temperature and completely disappears at $T^* \sim 140$ K (see Figs. 4a and 4b), even in the contact with the highest T_c . This temperature is strikingly close to the temperature at which long-range magnetic order appears in the parent, undoped compound²⁸. This fact naturally suggests the emergence of spin fluctuations from the progressive disruption of the AF long-range static order at the increase of x . The presence of the pseudogap also in the contact with the highest T_c indicates that AF spin fluctuations coexist with superconductivity even in optimally-doped $\text{LaFeAsO}_{1-x}\text{F}_x$.

The direct evidence here presented for the coexistence in the superconducting state of $\text{LaFeAsO}_{1-x}\text{F}_x$ of two order parameters – one superconducting and one possibly of magnetic origin – and a pseudogap related to spin fluctuations, together with other results in compounds of the same family¹⁴, demonstrates the strongly unconventional nature of superconductivity in Fe-As-based compounds and provides new hints for its theoretical understanding.

1. Parks, R. D. (Ed.) *Superconductivity*, CRC Press (1969).
2. Bennemann, K. H. & Ketterson, J. B. (Eds.) *The Physics of Superconductors*, Springer (2003).
3. Kamihara, Y. *et al.* Iron-based layered superconductor $\text{La}[\text{O}_{1-x}\text{F}_x]\text{FeAs}_x$ ($x = 0.05\text{--}0.12$) with $T_c = 26$ K. *J. Am. Chem. Soc.* **130**, 3296-3297 (2008).
4. Chen, X. H. *et al.* Superconductivity at 43 K in $\text{SmFeAsO}_{1-x}\text{F}_x$. *Nature* **453**, 761-762 (2008).
5. Ren, Z. A. *et al.* Superconductivity in iron-based F-doped layered quaternary compound $\text{Nd}[\text{O}_{1-x}\text{F}_x]\text{FeAs}$. *Europhysics Letters* **82**, 57002 (2008); Ren, Z. A. *et al.* Superconductivity at 55 K in iron-based F-doped layered quaternary compound $\text{Sm}[\text{O}_{1-x}\text{F}_x]\text{FeAs}$. *Chin. Phys. Lett.* **25**, 2215 (2008).

6. Boeri, L. *et al.* Is $\text{LaO}_{1-x}\text{F}_x\text{FeAs}$ an electron-phonon superconductor? *Phys. Rev. Lett.* **101**, 026403 (2008).
7. Mazin, I. I. *et al.* Unconventional sign-reversing superconductivity in $\text{LaFeAsO}_{1-x}\text{F}_x$. Preprint at <<http://arXiv.org/abs/0803.2740v3>> (2008).
8. Shan, L. *et al.* Unconventional pairing symmetry in iron-based layered superconductor $\text{LaO}_{0.9}\text{F}_{0.1-\delta}\text{FeAs}$ revealed by point-contact spectroscopy measurements. Preprint at <<http://arXiv.org/abs/0803.2405>> (2008).
9. Chen, T. Y. *et al.* A BCS-like gap in the superconductor $\text{SmFeAsO}_{0.85}\text{F}_{0.15}$. *Nature* **453**, 1224-1227 (2008).
10. Yates, K.A. *et al.* Point contact Andreev reflection spectroscopy of $\text{NdFeAsO}_{0.85}$. *Supercond. Sci. Technol.* **21**, 092003 (2008).
11. Samuely, P. *et al.* Unconventional superconducting order parameter(s) in $\text{NdFeAsO}_{0.9}\text{F}_{0.1}$? Probing by the point-contact Andreev-reflection spectroscopy. Preprint at <<http://arXiv.org/abs/0806.1672v2>> (2008).
12. Wang, Y. *et al.* Nodal Superconductivity with Multiple Gaps in $\text{SmFeAsO}_{0.9}\text{F}_{0.1}$. Preprint at <<http://arXiv.org/abs/0806.1986>> (2008).
13. Sato, T. *et al.* Superconducting Gap and Pseudogap in Iron-Based Layered Superconductor $\text{La}(\text{O}_{1-x}\text{F}_x)\text{FeAs}$. *J. Phys. Soc. Jpn.* **77**, 063708 (2008).
14. Ding, H. *et al.* Observation of Fermi-surface-dependent nodeless superconducting gaps in $\text{Ba}_{0.6}\text{K}_{0.4}\text{Fe}_2\text{As}_2$. Preprint at <<http://arXiv.org/abs/0807.0419>> (2008); Zhao, L. *et al.* Unusual Superconducting Gap in $(\text{Ba,K})\text{Fe}_2\text{As}_2$ Superconductor. Preprint at <<http://arXiv.org/abs/0807.0398>> (2008).
15. Alldredge, J. W. *et al.* Evolution of the electronic excitation spectrum with strongly diminishing hole density in superconducting $\text{Bi}_2\text{Sr}_2\text{CaCu}_2\text{O}_{8+\delta}$. *Nature Physics* **4**, 319-326 (2008).
16. Hasselbach, K., Kirtley, J. R. & Lejay, P. Point-contact spectroscopy of superconducting URu_2Si_2 . *Phys. Rev. B* **46**, 5826-5829 (1992); Escudero, R., Morales, F. & Lejay, P. Temperature dependence of the antiferromagnetic state in URu_2Si_2 by point-contact spectroscopy. *Phys. Rev. B* **49**, 15271-15275 (1994).
17. Lu, W. *et al.* Superconductivity at 41.0 K in the F-doped $\text{LaFeAsO}_{1-x}\text{F}_x$. Preprint at <<http://arXiv.org/abs/0804.3725>> (2008).

18. Gonnelli, R. S. *et al.* Direct evidence for two-band superconductivity in MgB₂ single crystals from directional point-contact spectroscopy in magnetic fields. *Phys. Rev. Lett.* **89**, 247004 (2002); Gonnelli, R. S. *et al.* Evidence for gap anisotropy in CaC₆ from directional point-contact spectroscopy. *Phys. Rev. Lett.* **100**, 207004 (2008).
19. Boris, A. V. *et al.* Signatures of Electronic Correlations in Optical Properties of LaFeAsO_{1-x}F_x. Preprint at <<http://arXiv.org/abs/0806.1732>> (2008).
20. Hunte, F. *et al.* Two-band superconductivity in LaFeAsO_{0.89}F_{0.11} at very high magnetic fields. *Nature* **453**, 903-905 (2008).
21. Singh, D. J. & Du, M. –H. Density functional study of LaFeAsO_{1-x}F_x: A low carrier density superconductor near itinerant magnetism. *Phys. Rev. Lett.* **100**, 237003 (2008).
22. Blonder, G. E., Tinkham, M., & Klapwijk, T. M., Transition from metallic to tunneling regimes in superconducting microconstrictions: Excess current, charge imbalance, and supercurrent conversion. *Phys. Rev. B* **25**, 4515 (1982).
23. Plecenik, A. *et al.* Finite-quasiparticle lifetime effects in the differential conductance of Bi₂Sr₂CaCu₂O_y/Au junctions. *Phys. Rev. B* **49**, 10016-10019 (1994).
24. Kashiwaya, S. *et al.* Theory for tunneling spectroscopy of anisotropic superconductors. *Phys. Rev. B* **53**, 2667-2676 (1996).
25. Nicol, E. J. & Carbotte, J. P. Properties of the superconducting state in a two-band model. *Phys. Rev. B* **71**, 054501 (2005).
26. Qiu, Y. *et al.* Neutron scattering study of the oxypnictide superconductor La(O,F)FeAs. Preprint at <<http://arXiv.org/abs/0805.1062>> (2008).
27. Luetkens, H. *et al.* Field and Temperature Dependence of the Superfluid Density in LaO_{1-x}F_xFeAs Superconductors: A Muon Spin Relaxation Study. Preprint at <<http://arXiv.org/abs/0804.3115>> (2008).
28. de la Cruz, C. *et al.* Magnetic order close to superconductivity in the iron-based layered LaO_{1-x}F_xFeAs systems. *Nature* **453**, 899-902 (2008); Dong, J. *et al.* Competing Orders and Spin-Density-Wave Instability in La(O_{1-x}F_x)FeAs. *Europhysics Letters* **83**, 27006 (2008).
29. Ishida, Y. *et al.* Evidence for Pseudogap Evolutions in High-Tc Iron Oxypnictides. Preprint at <<http://arXiv.org/abs/0805.2647>> (2008).
30. Held, K., Katanin, A. A. & Toschi, A. Dynamical vertex approximation – an introduction. Preprint at <<http://arXiv.org/abs/0807.1860>> (2008).

The authors wish to thank L. Boeri, R. De Renzi, O. Dolgov, S. Massidda, G. Sangiovanni, A. Toschi, for enlightening discussions. Special thanks to I.I. Mazin for kind advice, important comments and continuous encouragement.

Correspondence and requests for materials should be addressed to R. S. Gonnelli (renato.gonnelli@polito.it).

Figure 1 | Some examples of point-contact Andreev-reflection spectra as a function of temperature.

The raw conductance data shown in panels **a**, **b** and **c** were measured in three different point contacts, whose resistance is indicated in the panels, made on the same polycrystalline $\text{LaFeAsO}_{1-x}\text{F}_x$ sample. All the low-temperature spectra present two peaks, symmetric about zero bias, related to a smaller order parameter (OP) Δ_1 , and more or less pronounced shoulders (or peaks, in case **a**) related to a second, larger energy scale, Δ_2 . All these structures are indicated by arrows. The thick black line in each panel represents the normal-state conductance, and the corresponding temperature is to be considered as the critical temperature of the junction. The normal-state conductance shows a clear depression around zero bias, in a way similar to that observed by point-contact spectroscopy in URu_2Si_2 ¹⁶.

Figure 2 | Fit of normalized conductance curves as a function of temperature and magnetic field.

a Conductance curves of a point contact with $T_c=28.6$ K (the same as in Figure 1a) after normalization (symbols). The normal state at $T < T_c$, experimentally inaccessible, was here estimated by connecting the tails of the curve (at $|V| > 20$ meV) to a point at $V=0$, close to the zero-bias conductance at T_c , by means of a B-spline function (see Supplementary Information). Solid lines indicate the best-fitting theoretical conductance curves calculated with the generalized two-band BTK model. **b** Temperature dependence of the OPs Δ_1 and

Δ_2 , extracted from this fit (solid symbols), and of Δ_{peak} , value of the larger OP obtained in the hypothesis that its origin is not superconducting (open symbols). Δ_2 apparently follows a BCS-like curve up to ~ 22 K (but with a very high $2\Delta_2(0)/k_B T_c$ ratio), then either disappears or becomes so small to be undetectable. Δ_{peak} shows initially a modest increase and finally collapses above 22 K while Δ_1 is non-BCS and always shows a tail up to T_c . Dashed lines are guides to the eye. If the larger OP is not superconducting, its amplitude can be indicated by the energy of the peaks (open symbols) in the tunnelling contribution to the conductance (see panel e). **c** Magnetic-field dependence of the conductance curves (normalized as in panel a) of a point contact with $T_c=27.3$ K (see Fig.1c). All the measurements were taken at 1.8 K. Symbols represent experimental data, lines are the best-fitting curves. **d** Magnetic-field dependence of Δ_1 and Δ_2 extracted from the fit (solid symbols) and of the peak energy Δ_{peak} – to be intended as an alternative to Δ_2 in case the larger OP is not a superconducting one – (open symbols). Dashed lines are guides to the eye. **e** Temperature dependence of the normalized partial conductance, G_2^{tunn} due to plain tunnelling, extracted from data shown in panel a in the hypothesis that the large OP is not superconducting. The peak positions (indicated by arrows) are reported in panel b as open symbols.

Figure 3 | Fit of normalized conductance curves of a contact with the highest T_c and featuring only one order parameter.

a Conductance curves of a 15- Ω point contact with $T_c=31.0$ K after normalization, obtained as in fig. 2a (symbols). Solid lines indicate the best-fitting theoretical conductance curves calculated with the generalized single-band BTK model. At $T=1.8$ K the best-fitting parameters are: $\Delta=4.59$ meV, $\Gamma=3.27$ meV, and $Z=0.40$. **b** Temperature dependence of the OP extracted from this fit (solid symbols). The trend is definitely non-BCS and very similar to that shown in Fig.2b for Δ_1 . The dashed line is only a guide to the eye. **c** Magnetic-field dependence of the conductance curves (normalized as in panel a) of the same point contact. All the measurements were taken at 1.8 K. Symbols represent experimental data, lines are the best-fitting curves. **d** Magnetic-field dependence of the OP extracted from the fit of the curves shown in panel c. This behaviour is compatible with that

predicted for type-II superconductors, and with a critical field of the order of 55 T. **e** Values of Δ_1 , Δ_2 and Δ_{peak} obtained in different point contacts, reported as a function of the critical temperature of the contact. Error bars also take into account the different normalizations. The spread in T_c values is due to the fact that the sample presents homogeneous, large crystallites with various F concentrations embedded in a disordered matrix. The measurements show that Δ_1 is always close or below the BCS value (dashed black line) and increases with T_c , while Δ_2 and Δ_{peak} are well above the BCS line and decreases (with different slope) on increasing T_c , until a single BCS OP is observed.

Figure 4 | Pseudogap in the superconducting and normal state of $\text{LaFeAsO}_{1-x}\text{F}_x$.

Two examples of the temperature dependence of the conductance curves up to temperatures well above T_c . The first non-superconducting conductance curve is shown as a thick line and clearly features the zero-bias suppression already well visible in Fig.1. This “dip” or pseudogap, which progressively fills at the increase of temperature, is accompanied in many cases by two broad humps at energies much greater than both the OPs. This behaviour closely resembles that of point-contact conductance curves measured in URu_2Si_2 , that was ascribed to the presence of spin-density-wave order¹⁶. The whole curve is also asymmetric, probably reflecting the decrease in the DOS across the Fermi level. Moreover, the central dip disappears at temperatures of the order of 140 K, which is close to the temperature at which the magnetic long-range order appears in the undoped compound. In both panels a and b the first conductance curve that does not show any trace of zero-bias suppression or pseudogap is represented by a thicker line and the corresponding temperature is indicated in bold on the right.

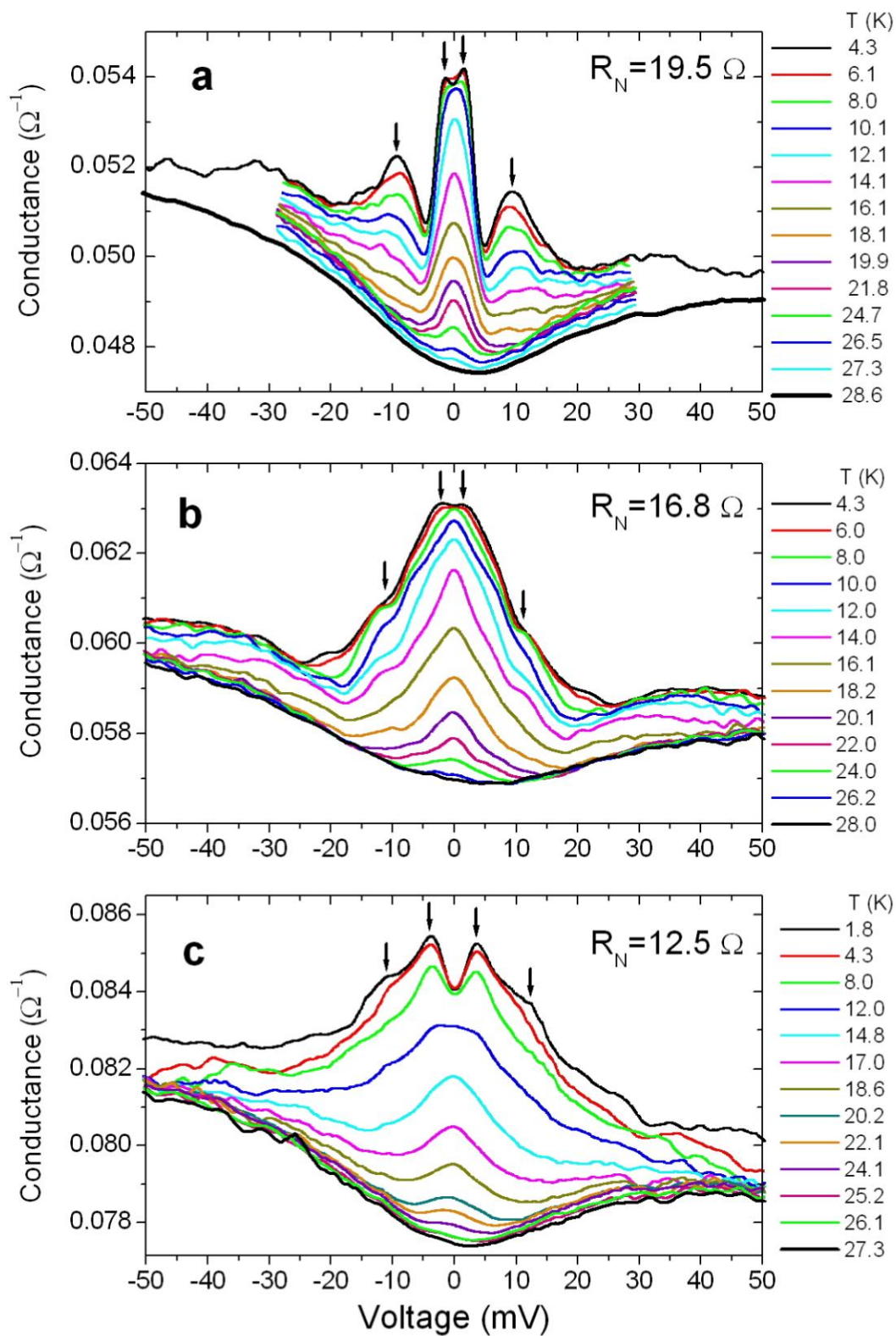


Figure 1 | Some examples of point-contact Andreev-reflection spectra as a function of temperature.

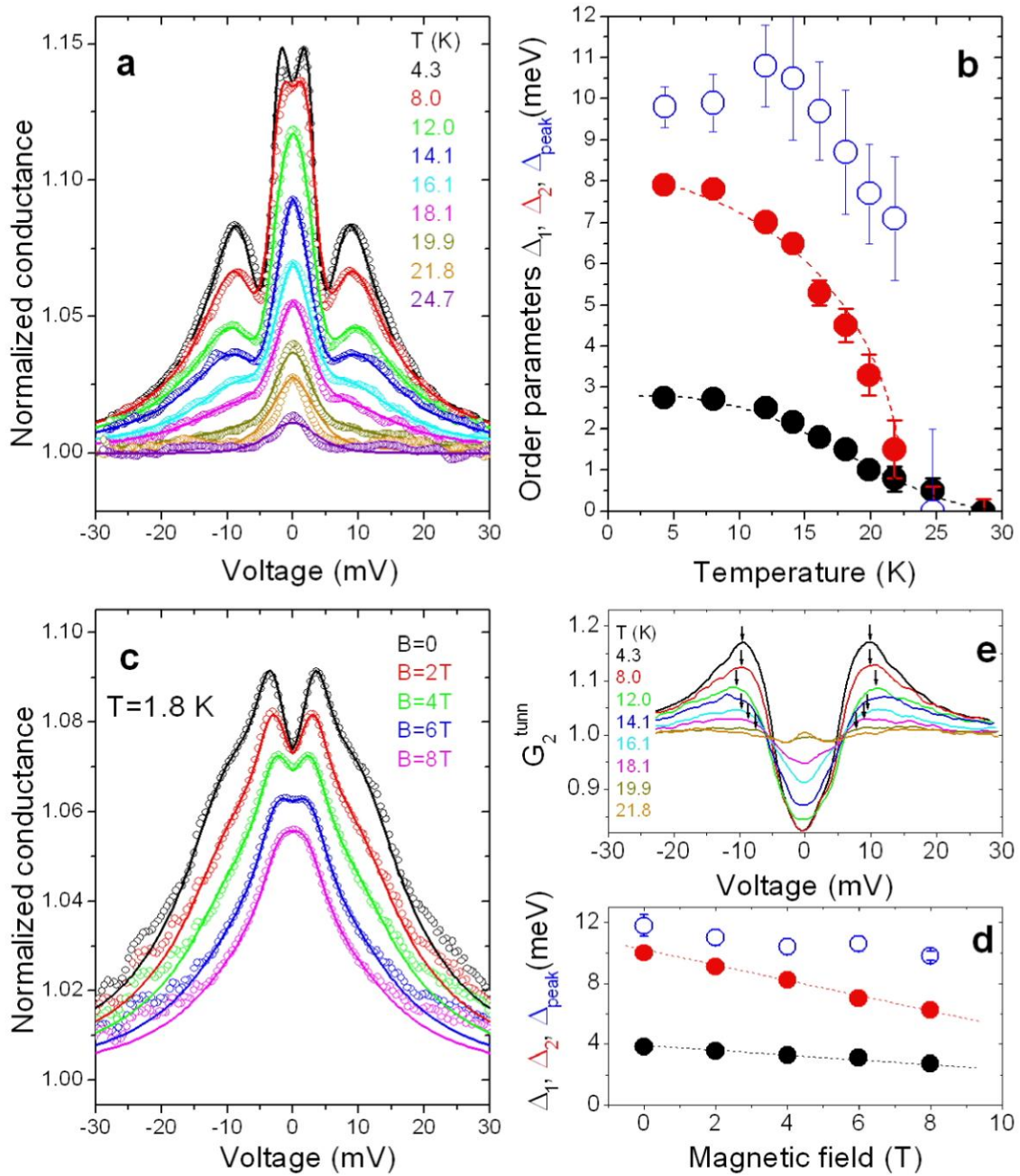


Figure 2 | Fit of normalized conductance curves as a function of temperature and magnetic field.

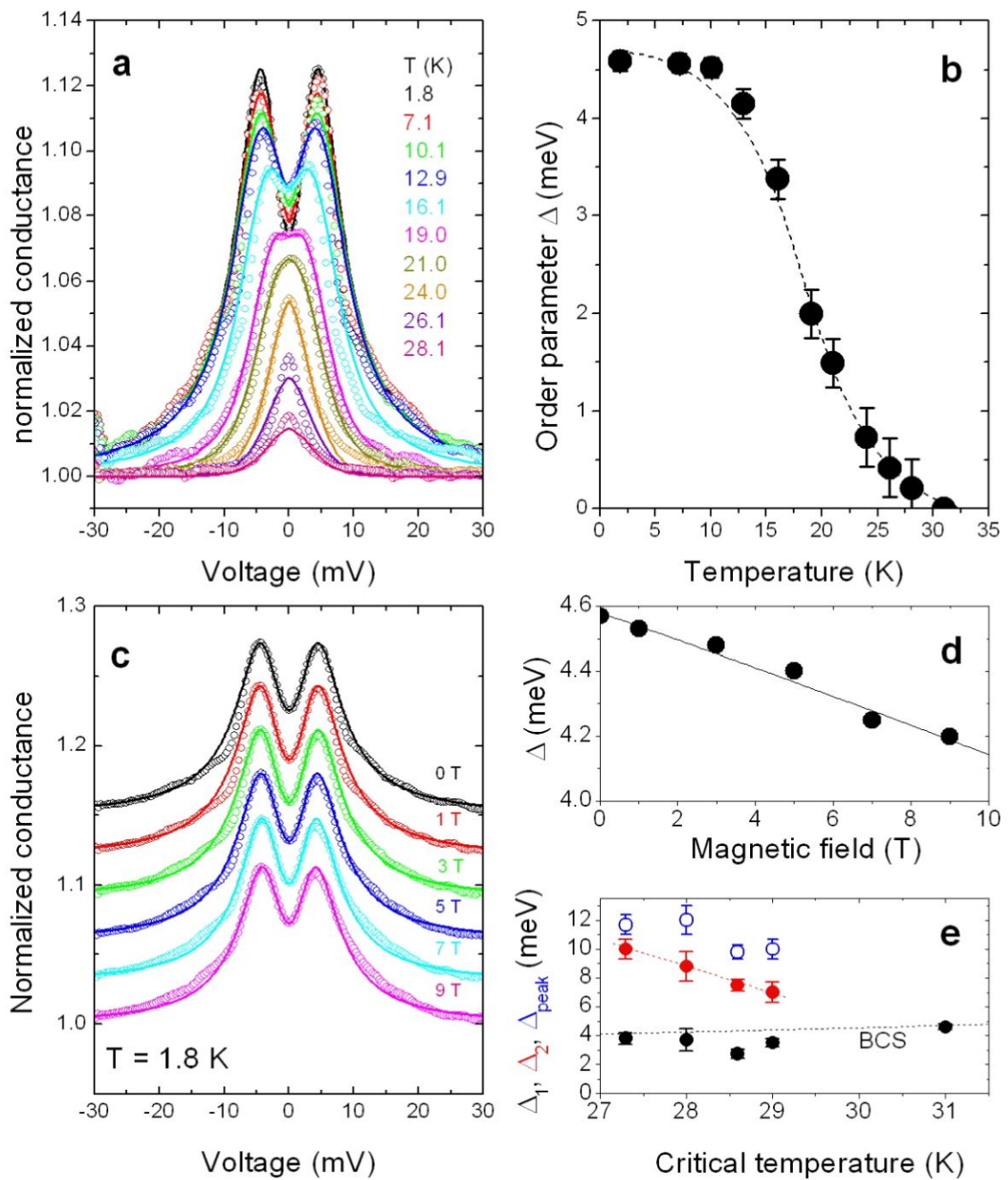


Figure 3 | Fit of normalized conductance curves of a contact with the highest T_c and featuring only one order parameter.

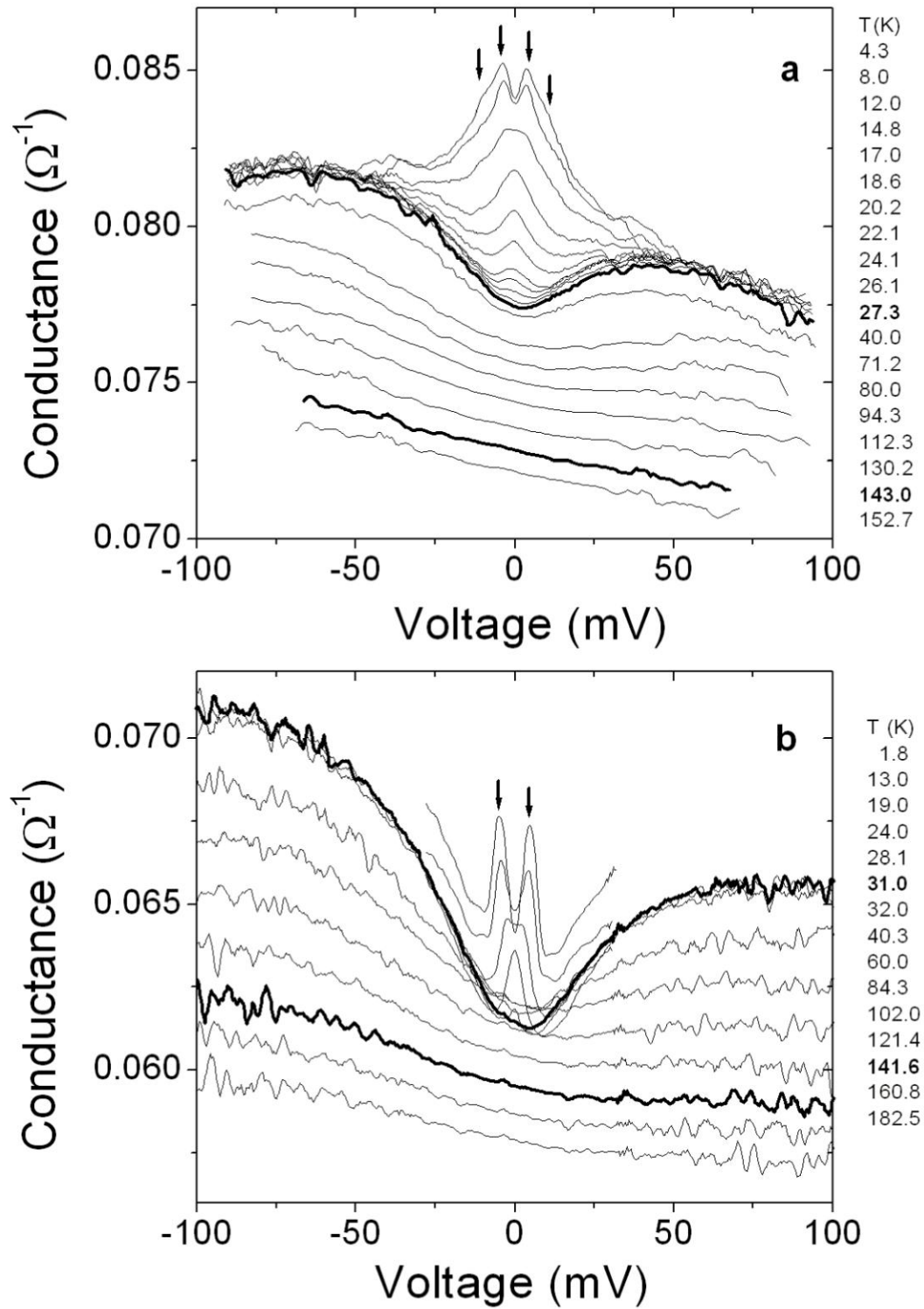
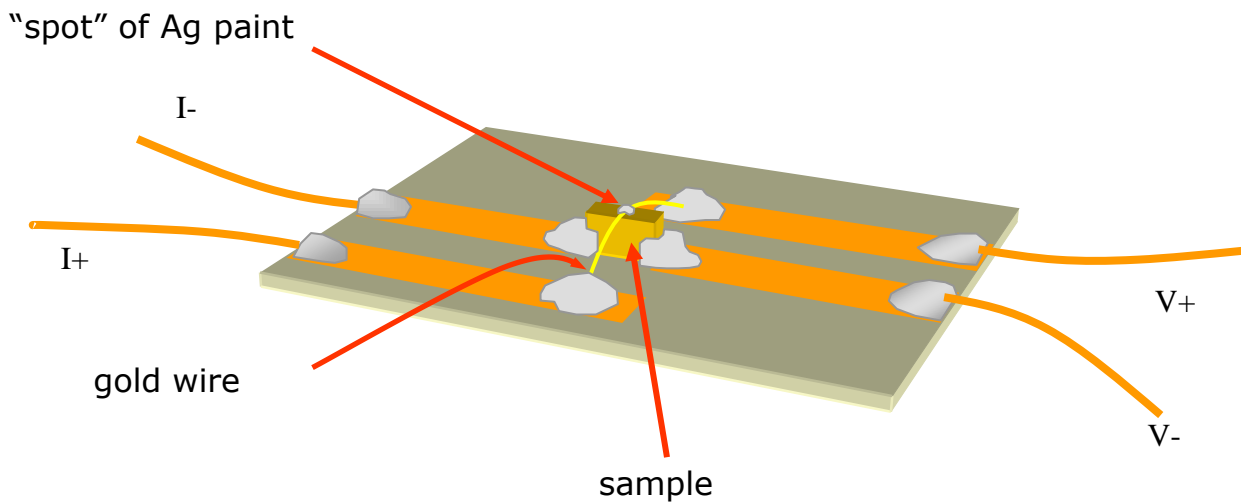


Figure 4 | Pseudogap in the superconducting and normal state of $\text{LaFeAsO}_{1-x}\text{F}_x$.

Supplementary Information

In this work we used a modified PCS technique in which the point contact between the superconductor and the normal metal is made by putting a small spot of Ag conductive paint (whose diameter is not greater than $50\ \mu\text{m}$) on the freshly exposed sample surface, instead of pressing a metallic tip against it as in standard PCS. This pressure-less technique can be used also on brittle or very thin samples, avoids the thermal drifts – that usually hinder the measurement of the conductance curves at high temperature – and gives a good repeatability of the measurements. The experimental set-up is schematized in Supplementary Figure 1. The voltage is defined to be negative when electrons are injected into the superconductor.



Supplementary Figure 1. Mounting of the sample with the Ag-paint spot and the current and voltage leads.

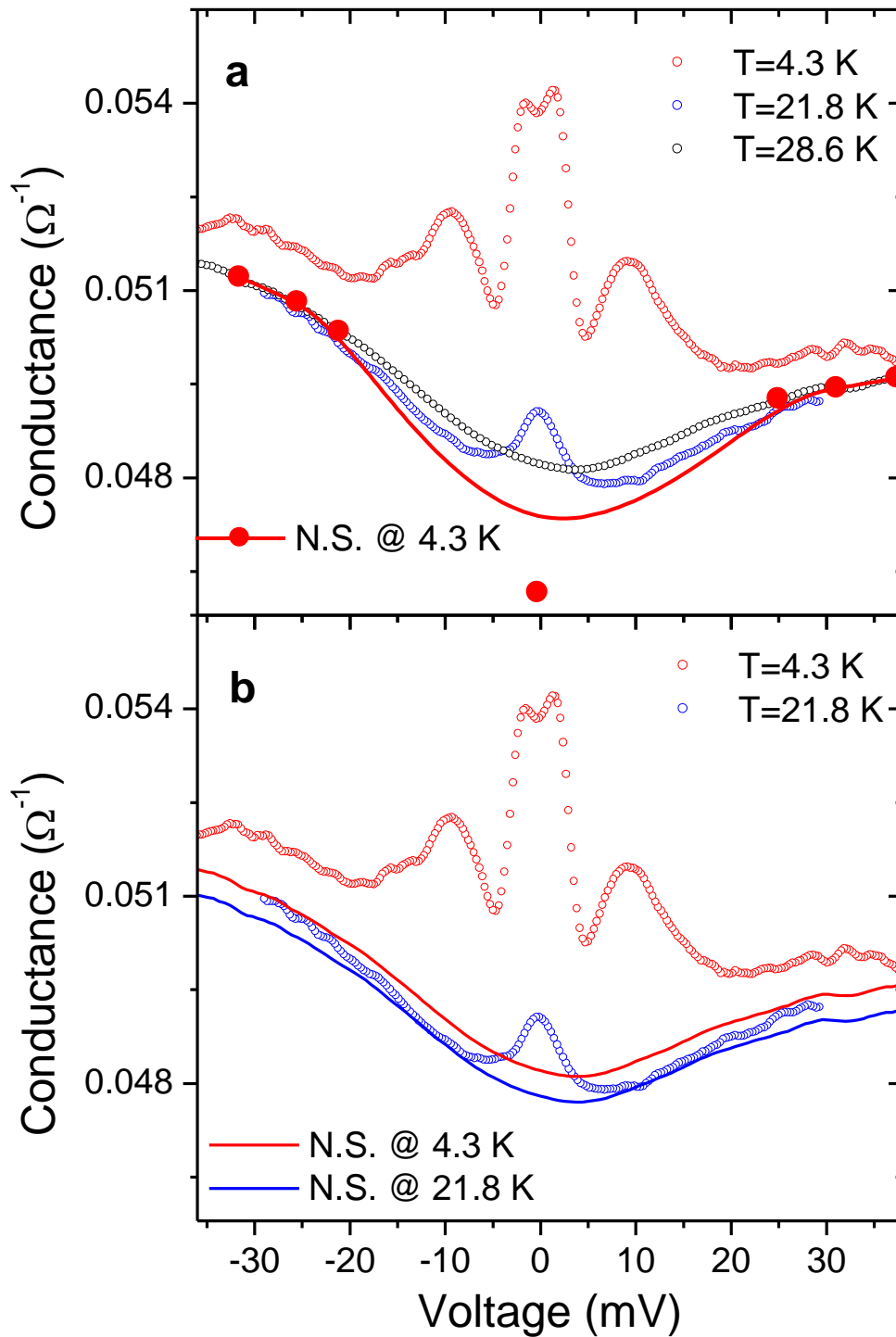
The contact resistance can be tuned by applying short voltage or current pulses to the junctions [18], but in general it is much smaller than in tunnel contacts, where an insulating barrier is interposed between normal metal and superconductor. In these conditions, if one of the banks is superconducting, the conduction through the junction is governed by the so-called Andreev reflection [31], that results in peaks or shoulders at voltages corresponding to the amplitude of the order parameter(s) in the superconductor. In performing PCS measurements, one should systematically check

that every junction fulfills the condition for ballistic transport in the contact – i.e. that the contact size a is smaller than the mean free path ℓ – so that charge carriers are not scattered in the contact area and are injected in the superconducting side with an excess energy eV , being V the voltage drop across the junction. Note that, in our case, the real contact between the Ag grains in the paint and the sample surface occurs on a nanometric scale and is thus orders of magnitude smaller than the diameter of the Ag spot [18]. Through the Sharvin formula for the normal-state resistance of a perfectly ballistic point contact,

$$R_N = \frac{4\rho\ell}{3\pi a^2}$$

the condition on the contact size ($a \ll \ell$) turns into a condition for R_N , which must exceed a minimum value related to ℓ . In our case, unfortunately, an evaluation of the real contact size a is impossible due to the lack of information about the mean free path in $\text{LaFeAsO}_{1-x}\text{F}_x$, and to the fact that using a simple free-electron model to estimate ℓ from the resistivity is a very rough approximation in a material with such a small density of charge carriers [21]. This problem is common to all the PCS measurements in oxypnictides appeared so far [8-12]. In these conditions, the reliability of the measurement can only be judged by looking at the shape of the conductance curves. If, as in our case, they do not show sharp dips nor a dome-shaped normal state conductance (both related to heating effects in the contact), substantial heating effects at the interface can be excluded and a ballistic conduction can be assumed.

The normalization of the conductance curves was performed in two different ways. Experiments clearly show that the shape of the normal state depends on temperature – the zero-bias dip, or pseudogap, being progressively filled on increasing temperature. This is evident above T_c , but can be inferred also in the superconducting state by looking at the tails of the conductance curves. Hence, we adopted two alternative choices for the normal state, exemplified in Supplementary Figure 2.



Supplementary Figure 2. Explanation of the two alternative choices for the normalization of the conductance curves. **a** The normal state at $T=4.3$ K is simulated by a “guess” curve (red line) obtained by connecting the red points with a B-spline function. In this way, the calculated “normal state” at 4.3 K is deeper than the measured normal state at T_c , respecting the progressive filling of the pseudogap suggested, for example, by the conductance curve at $T=21.8$ K (blue symbols). **b** All the curves are divided by the measured normal state at T_c (red line), translated if necessary (e.g. at $T=21.8$ K, blue line).

In panel (a) we report a subset of the full T dependence shown in Fig. 1a. By comparing the normal-state conductance at $T_c=28.6$ K (black symbols) to the curve at $T=21.8$ K (blue symbols) the progressive “filling” of the background (and the consequent increase of normal-state zero-bias conductance, NZBC) on increasing the temperature is clear. Therefore the normal state at $T=4.3$ K should coincide with that at T_c for $V>20$ mV, but should also feature a smaller NZBC. The red line, constructed by connecting the red points with a B-spline function, is a guess for that normal state and is the curve by which the experimental data at $T=4.3$ K were divided. The same procedure was used for the other temperatures, respecting the progressive increase in the NZBC. The results of the fit performed after this normalization were shown in Fig. 2a and are also reported for convenience in Supplementary Figure 3a as solid circles.

In panel (b) of Supplementary Figure 2, a different possible choice for the normalization is described. Here we simply used the normal-state conductance at T_c (vertically translated if necessary) to normalize all the curves. For example, the curve at $T=4.3$ K was divided by the normal state at T_c (red line) while the curve at $T=21.8$ K was divided by the normal state translated downward of a suitable amount (blue curve). This second procedure clearly gives rise to some anomalies in the points at high bias, where the normalized curves will depart from unity (the same happens in Ref. 9). The amplitudes of Δ_1 and Δ_2 obtained from the fit of the conductance curves normalized in this way are reported in Supplementary Figure 3a as open circles.

Despite the large difference in the normalization, at low temperature the amplitude of Δ_2 changes by less than 10% and that of Δ_1 by less than 1.5%.

The fit of the normalized curves, in the hypothesis that both the order parameters are superconducting, was performed by supposing that the conductance can be expressed as the sum of suitably weighted contributions

$$\text{SE1} \quad G = w_1 G_1^{BTK} + (1 - w_1) G_2^{BTK}$$

where each conductance is given (at $T=0$, for simplicity) by the Blonder-Tinkham Klapwijk model [22] generalized to the 3D case [24]:

$$\text{SE2} \quad G_i^{BTK}(E) = \frac{\int_{-\pi/2}^{\pi/2} \sigma_{S,i}(E, \phi) \cos(\phi) d\phi}{\int_{-\pi/2}^{\pi/2} \sigma_{N,i}(\phi) \cos(\phi) d\phi}$$

where $i=1,2$, ϕ is the angle the direction of injection makes with the normal to the interface, and

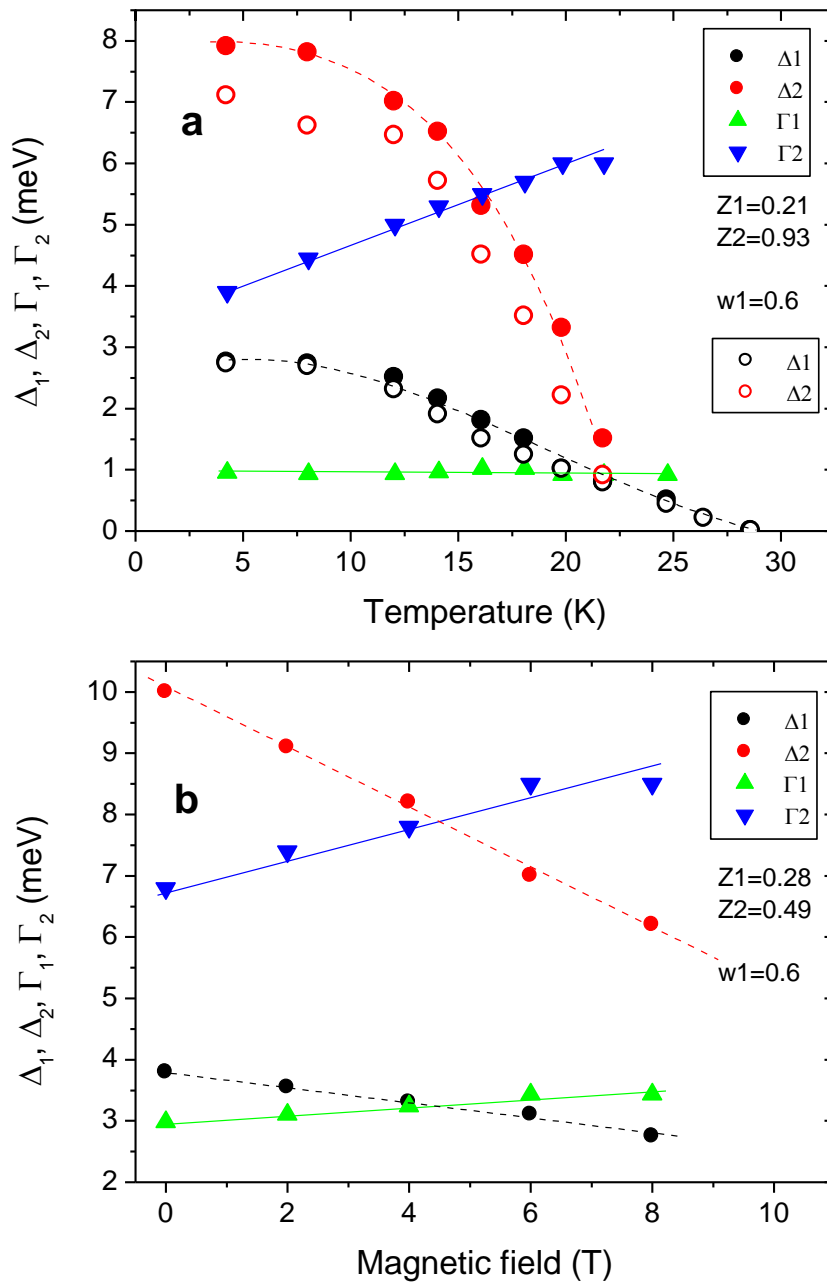
$$\text{SE3} \quad \sigma_{N,i}(\phi) = \frac{\cos(\phi)^2}{\cos(\phi)^2 + Z_i^2}$$

$$\text{SE4} \quad \sigma_{S,i}(E, \phi) = \sigma_{N,i}(\phi) \times \frac{1 + \sigma_{N,i}(\phi)|F_i(E)|^2 + (\sigma_{N,i}(\phi) - 1)|F_i(E)|^2}{|1 + (\sigma_{N,i}(\phi) - 1)F_i(E)|^2}.$$

where the parameters Z_1 and Z_2 are related to the height of the potential barrier at the interface. The functions $F_i(E)$ are given by

$$\text{SE5} \quad F_i(E) = \frac{(E + i\Gamma_i) - \sqrt{(E + i\Gamma_i)^2 - \Delta_i^2}}{|\Delta_i|}$$

and contain the order parameters Δ_1 and Δ_2 . As a further generalization, we included in the model the broadening parameters Γ_1 and Γ_2 as imaginary parts of the energy, E [23]. In our case, Γ_1 and Γ_2 account for both the (small) intrinsic lifetime broadening and other effects—related to the experimental technique and thus extrinsic—that smooth the curves and decrease the amplitude of the Andreev signal. Their values are always smaller than the corresponding OP amplitude, and increase on increasing temperature and magnetic field intensity. In the absence of theoretical indications, the weight w_I was taken as an adjustable parameter to be fixed by the fit. Actually, in most cases we got $w_I=0.6$. The parameters Z_1 and Z_2 that enter equation SE3 are related to the height of the potential barrier at the interface and are independent of both temperature and magnetic field. An example of the evolution of the fitting parameters as a function of temperature and magnetic field is reported in Supplementary Figure 3a and 3b. The data refer to the curves shown in Figure 2a and 2c, respectively.



Supplementary Figure 3. **a** Temperature dependence of the broadening parameters Γ_1 and Γ_2 obtained from the fit of the curves in Figure 2a, compared to the amplitude of the order parameters Δ_1 (full black circles) and Δ_2 (full red circles) obtained by the same fit. The values of Z_1 and Z_2 are temperature-independent and are indicated in the legend, together with the weight used in the fit. Open circles indicate the values of Δ_1 and Δ_2 given by the normalization described in Supplementary Figure 2b. The other fitting parameters are very little affected by the choice of the normalization. **b** Magnetic-field dependence of the broadening parameters compared to the OP amplitudes, as obtained from the fit of the curves in Fig. 2c. Z_1 and Z_2 were taken as being independent of the magnetic field; their values are indicated in the legend, with the weight w_1 .

If the larger OP is assumed not to be superconducting, the normalized conductance can be written as

$$\text{SE6} \quad G = w_1 G_1^{BTK} + (1 - w_1) G_2^{tunn}$$

where the first contribution is the usual generalized-BTK Andreev-reflection conductance, but the second one is the tunnel conductance into a DOS $N_2(E)$ which is not flat but contains structures determined by the larger OP:

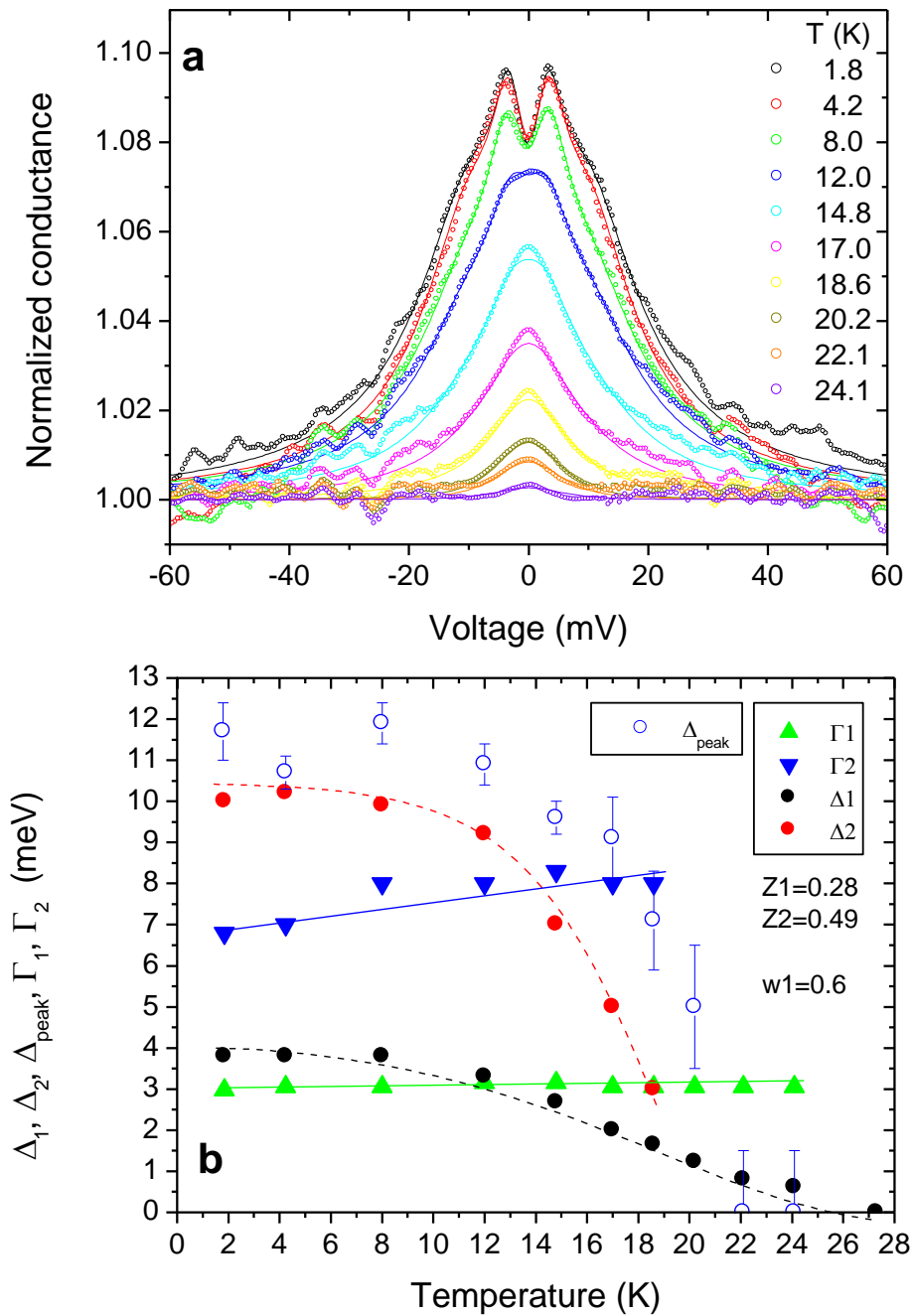
$$\text{SE7} \quad G_2^{tunn} = \int_{-\infty}^{\infty} N_{2,N}(E) \left[-\frac{\partial f(E + eV)}{\partial(eV)} \right] dE$$

where $N_{2,N}(E)$ is the normalized DOS and $f(E)$ is the Fermi function at the temperature at which the measurement was carried out. In principle, at $T=0$ the conductance G_2^{tunn} coincides with the normalized DOS, while at $T \neq 0$ it contains a thermal broadening term. The shape of the tunnel-conductance contribution G_2^{tunn} that best agrees with the experimental conductance G^{exp} curve is given by

$$\text{SE8} \quad G_2^{tunn} = \frac{G^{exp} - w_1 G_1^{BTK}}{1 - w_1}$$

and contains all the structures that are not related to the smaller OP, in particular clear peaks whose energy position (Δ_{peak}) changes on increasing the temperature or the magnetic field, as shown in Fig. 2b and 2d (open circles).

Supplementary Figure 4 (panel a) reports, as an additional example, the conductance curves of Fig. 1c, normalized according to the method described in Supplementary Figure 2a. The experimental data are compared to the relevant two-band generalized BTK fit (lines) and the corresponding fitting parameters are shown in panel b of the same figure. The same panel also reports for comparison the values of Δ_{peak} that provide a rough measure of the larger OP if it is supposed to be non-superconducting.



Supplementary Figure 4. **a** The conductance curves of Fig.1c after normalization with the method described in Supplementary Figure 2a (symbols) and the relevant best-fitting curves calculated within the two-band generalized BTK model (lines). **b** Temperature dependence of the order parameters (Δ_1 and Δ_2) and of the broadening parameters (Γ_1 and Γ_2). The values of Z_1 , Z_2 and of the weight w_1 are indicated in the legend. Open circles represent the energy of the peaks in the tunnelling contribution to the conductance, Δ_{peak} , that estimates the amplitude of the larger OP if it is supposed to be a non-superconducting order parameter.